Modelling Simul. Mater. Sci. Eng. **8** (2000) 261–268. Printed in the UK PII: S0965-0393(00)11953-9

Electron and positron states in amorphous $Ni_{0.4}Pd_{0.4}P_{0.2}$

D M C Nicholson†, P A Sterne‡, J C Swihart§, Jeffry Tran‖ and Yang Wang¶

† Oak Ridge National Laboratory, Oak Ridge, TN 37831-6114, USA
‡ Lawrence Livermore National Laboratory, Livermore, CA 94550, USA
§ Physics Department, Indiana University, Bloomington, IN 47405, USA
‖ Physics Department, Luther College, Decora, IA 52101, USA
¶ Pittsburgh Supercomputing Center, Pittsburgh, PA 15213, USA

Received 16 September 1999, accepted for publication 10 February 2000

Abstract. We performed local density calculations of the electronic and positron states for a 300-atom model of bulk amorphous $Ni_{0.4}Pd_{0.4}P_{0.2}$. The procedure for constructing the model and the resulting distribution of bond angles and free volume are described. Comparisons are made to experiment and to models of amorphous $Ni_{0.8}P_{0.2}$.

0. Introduction

Bulk amorphous metals are an interesting class of new materials possessing unique properties that offer exciting possibilities for applications to a broad range of technologies. In contrast to the previous generation of amorphous metals, bulk amorphous metals can be produced in *bulk* form at cooling rates as low as $\sim$1 K s^{-1}. The understanding of their structure, is important to the explanation of their low cooling rate. One of the simplest and most studied bulk amorphous metal is $Ni_{0.4}Pd_{0.4}P_{0.2}$ [1]. We can benefit from the earlier work of Weber and Stillinger [2] who developed interatomic potentials for the conventional metallic glass $Ni_{0.8}P_{0.2}$ that were constructed specifically to reproduce the measured partial pair distribution functions (PDFs) [3]. Structures generated using these potentials have been used as the basis for density functional calculations of the electronic conductivity, density of electronic states, atomic density, and optical reflectivity [4]. The agreement of these calculations with experiment validates the atomic models and the interatomic potentials used in their construction. Recent measurements of the PDF and the Pd distribution function of $Ni_{0.4}Pd_{0.4}P_{0.2}$ [5] provide a very useful guide for extending the potentials of Weber and Stillinger [2] to the ternary alloy $Ni_{0.4}Pd_{0.4}P_{0.2}$. We describe the use of these potentials to generate a 300-atom unit cell model of amorphous $Ni_{0.4}Pd_{0.4}P_{0.2}$. We have confidence in our model because it reproduces the measured partial distribution functions, and electronic and positron states calculated with this model agree with photo-emission and positron lifetime measurements. The calculations of the electron and positron states were performed using the first-principles, order-N, locally self-consistent multiple scattering (LSMS) method [6]. We analysed the structure to determine the distribution of bonds, free volume, electronic states, and positron states. Comparisons were made to models of the conventional amorphous metal, $Ni_{0.8}P_{0.2}$. The most striking contrast is in the amount and distribution of free volume. Because free volume is so closely related to diffusion and the kinetics of glass stability it may be the key to the glass forming ability of $Ni_{0.4}Pd_{0.4}P_{0.2}$.

 © 2000 IOP Publishing Ltd

1. Computational technique: the LSMS method

The electronic structure of systems with a number of atoms, N in the unit cell as large as 300 cannot be obtained by conventional band structure methods. The LSMS method is an $O(N)$ multiple scattering method that is specifically designed for massive parallel processors [6]. It relies on several stationary properties of density functional theory to ensure accurate free energy determination based on an electron density that is determined self-consistently at each site [7]. The LSMS method makes the simplifying assumption that, for the purpose of solving the Schrödinger equation, the effective potential beyond a cluster of neighbouring atoms (the local interaction zone (LIZ)) surrounding each atom can be approximated by a constant. Each atom is then taken to be at the centre of its own LIZ. In the calculations presented here the atomic potentials are taken to be spherical and are obtained self-consistently within the atomic-sphere-muffin-tin approximation [8]. The LIZ is taken to be a sphere of radius 10 Bohr radii.

2. Atomic model

The calculations were performed for a periodically reproduced cubic box containing an amorphous network consisting of 300 atoms for which the atomic positions had first been relaxed to a local energy minimum via two-body interactions [4].

The starting point for generating the amorphous configurations was a previously published [4] structure for amorphous $Ni_{0.8}P_{0.2}$. This configuration was generated by random packing, followed by interchanges to eliminate P–P neighbours, and finally relaxation via the pair potentials of Weber and Stillinger. The $Ni_{0.8}P_{0.2}$ model structure has PDFs that agree well with experiment. We have considerable confidence in this structure because it has been used as the basis for many calculations that agree with experiment. However the algorithm that eliminated P–P nearest neighbours only frees the sample of P–P pairs that are closer than the smallest Ni–Ni distance. To remedy this weakness, without completely abandoning this model that has served us well, we scaled 'r' by a factor of 0.5 in the P–P potential in order to force greater P–P separation. We also made a very small adjustment to the Ni–P potential. This left the model substantially intact, but pushed those few closely-spaced phosphorus pairs to positions clearly identifiable as second nearest neighbours. The Pd-containing structure was then generated by randomly replacing half of the Ni by Pd. We then relaxed the structure using Ni–Pd, Pd–Pd, and Pd–P potentials introduced to augment the already defined Ni–Ni, Ni–P, and P–P potentials. The newly-introduced potentials were adjusted to optimize agreement with the measured partial distribution functions. The potentials are of the form

$$V_{ij}(R) = C_{ij}\, \mathrm{e}^{(\alpha_{ij}R-1.652\,194)^{-1}}[(\alpha_{ij}R)^{-12} - 1)\Theta(1.652\,194 - \alpha_{ij}R) \qquad (1)$$

with the parameters as given in table 1. $\Theta(x)$ is the heaviside function. The PDFs from the model are compared to the measured values [5] in figure 1.

Table 1. Parameters for potentials. Units: α is in units of inverse fcc Ni–Ni distance of 2.49 Å and C is in 10^{-12} ergs.

	Ni–Ni	Ni–Pd	Ni–P	Pd–Pd	Pd–P	P–P
C_{ij}	1.134	1.172	1.701	1.211	1.7011	0.567
α_{ij}	1.000	0.900	1.080	0.850	0.950	0.755

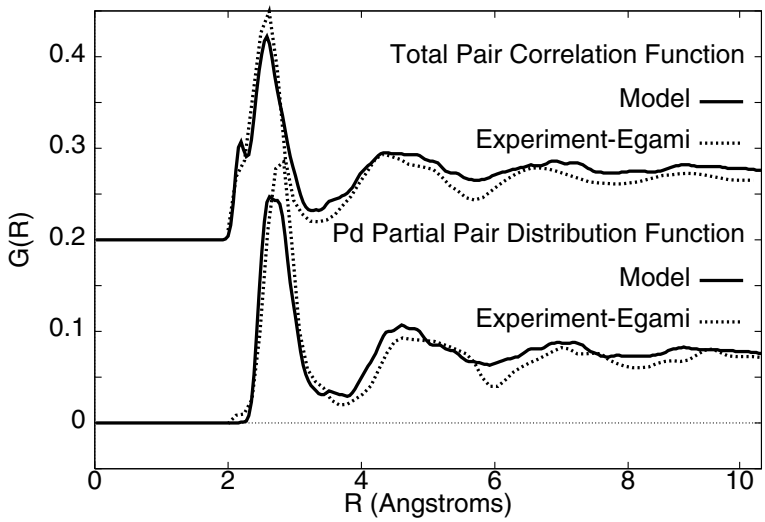

Figure 1. Comparison of model (full curves) amorphous pair distribution functions to measurements by Egami *et al* [5] (broken curves).

3. Stability and diffusion

Like many metallic glasses $(Ni_xPd_{1-x})_{0.8}P_{0.2}$ alloys are associated with a deep eutectic. A reasonable assumption is that at compositions where the liquid state is stable at unusually low temperatures the amorphous phase, which is essentially a frozen liquid, has a free energy competitive with alternative crystalline phases. If long diffusion paths are required to reach energetically-favoured crystalline structures, or if diffusion barriers are high, the conditions for glass formation are enhanced.

In crystals, the diffusion rate is controlled by the density of vacancies and the hopping time. The hopping time depends on the height of the barrier to vacancy hopping. In glasses the definition of a vacancy is not clear cut. Sietsma and Thijsse [9] have made progress toward a workable definition of a vacancy in glass. They characterize the unoccupied regions in the glass system according to their volumes and number of surrounding atoms. They observe that annealing eliminates large, local, free-volume elements that have greater than nine surrounding atoms. These large volumes, which tend to anneal out, are considered to play the role of vacancies, while those that remain are thought to be similar to interstitial sites or constitutional vacancies in crystals. The large and small volumes are referred to as holes and voids, respectively. The distribution of free volume, because it dominates diffusion is likely to play an important role in the kinetic stability of the glass.

We attempt to extend the understanding of the free volume in two ways. First, because our model is based on matching the measured PDFs, there is the hope that it also reproduces characteristics of the distribution of free volume found in the experimental sample. Hence, we study the distribution of free volume in our model. Although the PDFs do not uniquely determine the atomic arrangement, they do constrain it considerably and the distribution of free volume in our model may be indicative of its distribution in a real sample. Second, we study positron wavefunctions. Because positrons are repelled by the nuclei, injected positrons spend most of their time meandering through the interstitial regions and vacancies until they annihilate. If defects that trap the positrons are plentiful, the majority of positrons

will diffuse through the system for only a short time before being trapped. Once trapped they find themselves in a region of low electron density and have an extended lifetime characteristic of the type of defect (i.e. in a crystal typical traps would be monovacancies and divacancies). We take the initial steps necessary for interpreting the information available in the annihilation photons; we calculate the positron density and lifetime.

4. Atomic structure

We can further analyse the structure by tabulating distributions of bond angles. We find that the distribution of angles (figure 2) in $Ni_{0.4}Pd_{0.4}P_{0.2}$ is very similar to the distribution in $Ni_{0.8}P_{0.2}$. They both peak near $\theta = 60^\circ$ and 108° characteristic of icosahedral packing and differ only in small details. Fcc packing would have had peaks at 60°, 90°, and 120°. The population of bond angle can be subdivided according to whether the vertex atom is phosphorus or transition metal and the number of phosphorus atoms among the remaining two atoms that form the angle. The angle populations involving only transition metal atoms at the two compositions are very similar and are very icosahedral in nature. The angles with a P vertex have very similar distributions at the two compositions; the angles are predominately around 70°, consistent with a lower coordination around P. The case of a transition metal vertex and a P and transition metal atom completing the angle shows the greatest change with composition. This change is because Pd and Ni sit at different distances from the phosphorus due to their different sizes. The angles formed by a transition metal atom at the vertex and two phosphorus atoms are distributed in a broad peak (not shown) centred at 100° with no angles below about 80° because there are no P–P nearest neighbours.

Another way of describing the bonds is to look at the atoms surrounding each bond. In a perfectly icosahedral system each bond would have five surrounding atoms that are common

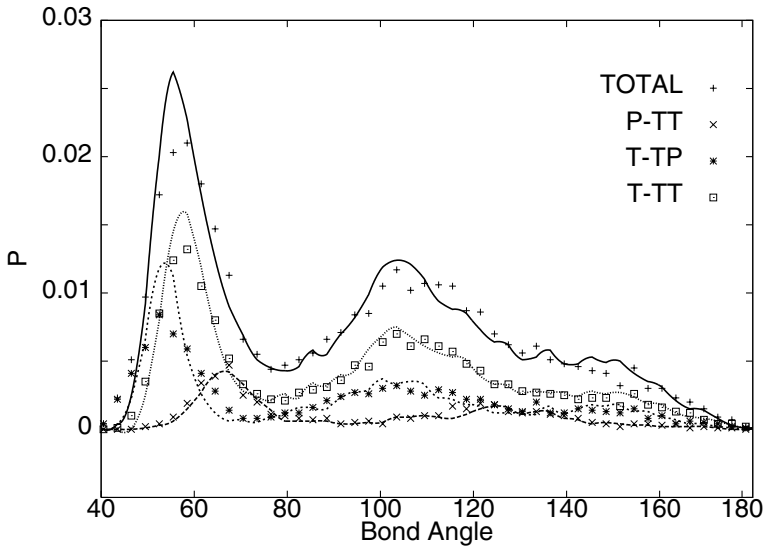

Figure 2. The distribution of bond angles: the curves denote results for $Ni_{0.8}P_{0.2}$; the solid curve is for all bond angles, the long-dash curve is for the P-vertex bonding to two Ni, the short-dash curve is for the Ni-vertex bonding to a P and a Ni, the dotted curve is for all Ni. The symbols apply to $Ni_{0.4}Pd_{0.4}P_{0.2}$ and are labelled in the key, T stands for Ni or Pd. For example, P–TT stands for a phosphorus-vertex bonding with two transition metal atoms.

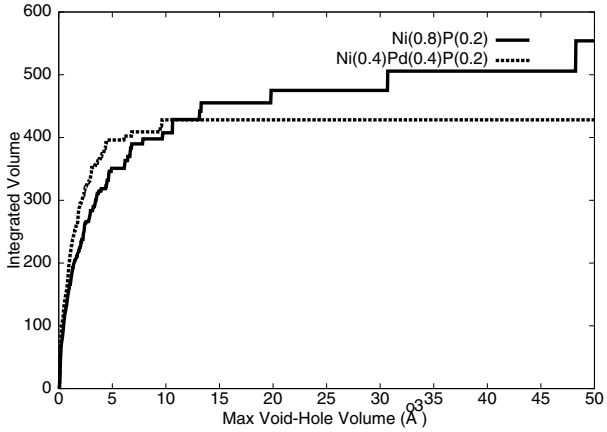

Figure 3. The integrated distribution of free volumes: $Ni_{0.8}P_{0.2}$ is denoted by a full curve and $Ni_{0.4}Pd_{0.4}P_{0.2}$ is denoted by a broken curve.

nearest neighbours to the two atoms that form the bond. Fcc would have four bond neighbours. In our models we find that the most commonly occurring number of bond neighbours is five. About half the bonds have five bond neighbours, with the remaining bonds having numbers of neighbours predominately in the ranging from four to seven. For transition metal bonds about four of the surrounding atoms are transition metal atoms and one is P. The bonds with more than five neighbours usually have an additional P. Again, there is no clear-cut distinction between the two systems. From the point of view of bonds the structure behaves substitutionally, with local dilation to account for the larger size of Pd, but on average preserving the bond angles. This is consistent with the observation made by Egami *et al* [5]: that the PDFs are roughly concentration independent; and the observation of Alamgir *et al* [10]: that the core levels are roughly concentration independent. It is doubtful that these small differences in bond statistics can be held accountable for the much greater glass forming ability of $Ni_{0.4}Pd_{0.4}P_{0.2}$.

Another way to characterize the atomic structure is to look where the atoms are not. We construct Voronoi polyhedra [11] according to the radical plane construction [12] using the radii 2.293, 2.66, and 1.963 au for Ni, Pd and P, respectively. We then shift our attention to the points farthest from the atoms, the vertices of the Voronoi polyhedra. These are the points associated with the free volume [9]. For each vertex we find the largest sphere that does not overlap any atomic sphere. We then group those vertex-centred spheres that overlap each other. The space defined by the overlapping, vertex-centred spheres defines a cell of free volume. The distribution of the volumes of these cells is shown in figure 3. The figure shows the integrated free volume (i.e. the sum of all free volume below a limiting void or hole size). There are two major differences between the two compositions. The Pd-containing composition has less free volume and less of the free volume is associated with large-volume cells. This could be a manifestation of the higher packing fraction possible with a distribution of atomic sizes.

In bulk amorphous alloys, as proposed by Sietsma and Thijsse, diffusion is probably controlled by the large free volumes, holes, that are smaller than vacancies but larger than the interstitial volumes in ordered materials. Reduction of the number of these holes may be the mechanism by which bulk amorphous alloys are prohibited from diffusive transformation to the crystalline ground state even when cooled slowly. It would be valuable to have measured values for the positron lifetimes at these two compositions. The validity of our model free-volume distributions would be supported if the lifetime was longer for $Ni_{0.8}P_{0.2}$, indicating that the more plentiful holes trapped the positrons.

5. Positron states

Positrons are trapped by defects, particularly vacancies. When they annihilate they provide information about the electron density at the defect as well as the atomic species of surrounding atoms. In a simple system, such as well annealed Cu with a few well dispersed monovacancies, two lifetimes are observed. One is a short lifetime associated with itinerant positrons in the bulk, and the other is a longer lifetime associated with positrons trapped at the vacancies. The density of vacancies and the electron density at the vacancy site can be determined. In more complex systems there may be one lifetime, or several lifetimes. For example, amorphous metals typically have one broadened lifetime, the interpretation of which is not clear. It is still debatable whether all annihilation is of the bulk type or from defects. In these more complex systems models are needed to extract useful information from the positron experiments.

The two photons created when a positron annihilates with an electron carry away the momentum and energy of the pair. Because the positrons have (shortly after injection) only thermal energies, a high-momentum photon pair indicates annihilation with a high-momentum core electron, rather than a low-momentum valence electron. The high momentum part of the core annihilation profile as a function of momentum is characteristic of the element and can be obtained by experiments on the pure element and by calculation [13]. In multicomponent systems, the high momentum profile of positrons trapped in vacancies can be compared to profiles from the pure elements to indicate the atomic number of the atom whose core electron participated in the annihilation [13]. The simplest assumption is that the atoms participating in the annihilation are nearest neighbours of the trapping defect.

At this stage we can calculate the positron wavefunctions and determine which nuclei have the greatest overlap with the positron density. We did this by calculating the electrostatic potential of our self-consistent electron density. The local approximation to the electron–positron correlation potential [14] was added to the electrostatic part to provide a one-particle Schrödinger equation for the positrons. We used the LSMS to solve for the positron wavefunctions. The site decomposed density of states shows that the low-energy positrons are predominately on P sites. The product of the electron and positron densities adjusted for correlation and multiplied by the annihilation cross section gives the positron annihilation rate [14]. We have not yet incorporated the matrix elements that couple the positron wavefunctions to the electronic core levels. Therefore, we cannot predict the characteristic patterns that will be seen in high-momentum positron annihilation experiments on $Ni_{0.4}Pd_{0.4}P_{0.2}$ when they are carried out. We have observed that the positrons have their greatest overlap with the phosphorus core so we can anticipate that the high-momentum annihilation will indicate annihilation at phosphorus cores.

We can compare our calculated positron lifetime to some interesting preliminary measurements by Somieski [15] of the positron lifetime in $Ni_{0.4}Pd_{0.4}P_{0.2}$. Their measurements give lifetimes in an as-quenched specimen distributed in the range 140–180 ps [15]. After annealing for 24 h at 200 °C a second group of lifetimes appears in the range 100–120 ps. Our calculated average lifetime for the lowest eight positron states is 114 ps. One possible explanation of these results is that the as-quenched sample has large defects similar to quenched-in thermal vacancies in rapidly-cooled crystals. These defects in the amorphous structure may have long lifetimes in the 140–180 ps range. These defects could have large trapping cross sections that could account for nearly all annihilation events. In the computer-generated model these large vacancies are probably precluded by the model construction procedure. When the experimental sample is annealed, the number of large vacancies is reduced and eventually the smaller-free-volume cells similar to those seen in the model begin to trap positrons with sufficient probability to be observed in the experiments in the range 100–120 ps.

6. Electronic states

The electronic density of states is modified considerably by the addition of Pd (figure 4). Substitution of Pd for Ni greatly increases the overall d-band width of $Ni_{0.4}Pd_{0.4}P_{0.2}$ relative to $Ni_{0.8}P_{0.2}$ [4]. This occurs because of the broader d-band width of elemental Pd and because the centres of the Ni and Pd d-bands are displaced from each other. The Ni states occupy the upper part of the band and the Pd states dominate in the lower part of the band. This separation is seen in the behaviour of the x-ray photo-emission spectrum (XPS) as a function of Pd concentration [10].

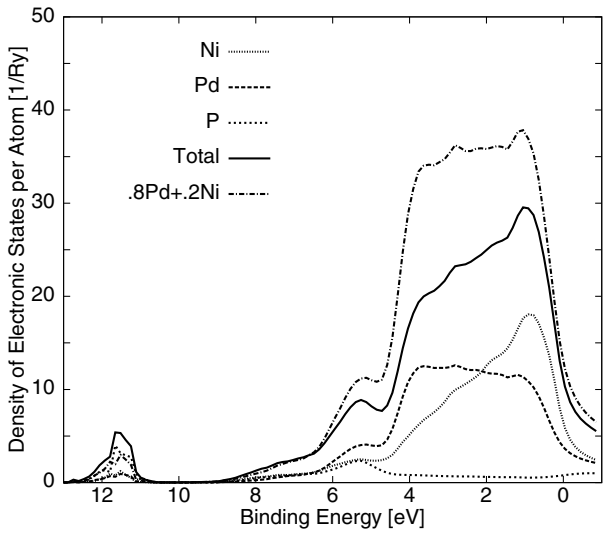

Figure 4. Density of states as function of electron energy for amorphous $Ni_{0.4}Pd_{0.4}P_{0.2}$; the zero of the energy scale is the Fermi energy. The dash–dot curve is the XPS calculated using a rough approximation to the inclusion of matrix elements (arbitrary units).

There is a long tail of states below the d-band that are contributed equally from Ni, Pd, and P states. From our experience with Ni–P we speculate that these tail states are somewhat localized due to the disorder. The fact that all species contribute equally to these tails would tend to make them independent of composition. This can be seen in the lack of composition dependence of the XPS data between 5 and 8 eV.

We find low-lying phosphorus states split-off from the d-bands. These states may be responsible for the barely perceptible bulge in the XPS data at a binding energy of 12.5 eV.

Our calculated density of states at the Fermi energy is higher than that seen in the XPS. Furthermore, we did not see a minimum in the density of states near the Fermi energy that, if present, would have indicated the effects of the stabilizing mechanism suggested by Nagel and Tauc [16]. Our density of states has a dip at 4.5 eV that is not seen in the XPS. A further difference between the density of states and the XPS is that the XPS d-band is almost symmetric about the band centre, while the calculation shows a strong Ni peak at the upper d-band edge. In order to show how inclusion of matrix elements affect the agreement, we plotted the weighted sum of the Ni and Pd densities of states. We weighted the Pd states by a factor of four relative to the Ni states. This is based on the statement of Almagir *et al* [10] that the P matrix element is very small and the matrix element for Pd is four times as large as for

Ni. This rough approximation to a true calculation [17] of the XPS gives excellent agreement with the measured spectrum.

7. Conclusions

We have used the PDFs recently measured by Egami *et al* [5] to develop interatomic potentials suitable for Ni–Pd–P amorphous alloys. We do not make any claim for the usefulness of the energy comparisons based on these potentials. Combined with the procedure of randomly packing hard spheres they should be viewed as part of an interpolation or extrapolation procedure that can use the PDFs of $Ni_{0.8}P_{0.2}$ and $Ni_{0.4}Pd_{0.4}P_{0.2}$ to construct models at other compositions. The geometric properties of the model are discussed along with the resulting electron and positron states. The comparisons of the electronic density of states and positron lifetimes with measurements are promising. These comparisons are not straight forward and there are additional questions to be addressed; still, it is fair to say at this stage that there are no contradictions that discredit the validity of our model structure.

Acknowledgments

Electronic and positron state calculations were performed at the Center for Computational Science at ORNL and the Pittsburgh Supercomputing Center. Work sponsored by ORNL Laboratory Directed Research and Development Fund, BES–DMS, and OCTR–MICS US Department of Energy under subcontract DEAC05-96OR22464 with Lockheed-Martin Energy Research Corporation. This work was also performed under the auspices of the US Department of Energy by the Lawrence Livermore National Laboratory under contract W-7405-ENG-48.

References

[1] He Y, Schwarz R B and Archuleta J I 1996 *Appl. Phys. Lett.* **69** 1861
Schwarz R B and He Y 1997 *Proc. Int. Symp. on Metastable, Mechanically Alloyed and Nanocrystalline Materials* (Los Alamos, NM: Los Alamos National Laboratory) Publication LA-UR-96-1703
[2] Weber T W and Stillinger F H 1985 *Phys. Rev.* B **31** 1954–63
[3] Lamparter P and Steeb S 1985 *Rapidly Quenched Metals* ed S Steeb and H Warlimont (Amsterdam: Elsevier) pp 459–68
[4] Yang H, Swihart J C, Nicholson D M and Brown R H 1993 *Phys. Rev.* B **47** 107–14
Yang H, Swihart J C, Nicholson D M and Brown R H 1993 *Materials Theory and Modeling (Mater. Res. Soc. Symp. Proc. vol 291)* ed J Broughton, P D Bristowe and J M Newsam, pp 419–24
[5] Egami T, Dmowski W, He Y and Schwarz R B 1998 *Met. Mater. Trans.* A **29** 1805
[6] Wang Y, Stocks G M, Shelton W A, Nicholson D M C, Szotek Z and Temmermann W M 1995 *Phys. Rev. Lett.* **75** 2867–70
[7] Nicholson D M C, Stocks G M, Wang Y, Shelton W A, Szotek Z and Temmerman W M 1994 *Phys. Rev.* B **50** 14 686–9
[8] Zhang X-G and Nicholson D M C 1999 *Phys. Rev.* B **60** 4551
[9] Sietsma J and Thijsse B J 1995 *Phys. Rev.* B **52** 3248
[10] Alamgir F M, Jain H, Miller A C, Williams D B and Schwarz R B 1999 *Phil. Mag.* B **79** 239
[11] Yang Wang and Stocks G M 1994 *Phys. Rev.* B **49** 5028
[12] Watson R E and Bennett L H 1991 *Phys. Rev.* B **43** 11 642
[13] Asokakumar P *et al* 1996 *Phys. Rev. Lett.* **77** 2097
[14] Sterne P A and Kaiser J A 1991 *Phys. Rev.* B **43** 13 892
[15] Bertram Somieski 1998 Oak Ridge National Laboratory, unpublished results
[16] Nagel S R and Tauc J 1975 *Phys. Rev. Lett.* **35** 380
[17] Winter H, Durham P J, Temmerman W M and Stocks G M 1986 *Phys. Rev.* B **33** 2370